

ORIGINAL PAGE IS
OF POOR QUALITY

N88-15619³¹⁸⁻⁷⁶
116720
298

1987

NASA/ASEE SUMMER FACULTY RESEARCH FELLOWSHIP PROGRAM

MARSHALL SPACE FLIGHT CENTER
THE UNIVERSITY OF ALABAMA IN HUNTSVILLE

A NUMERICAL STUDY OF TRANSIENT HEAT AND MASS TRANSFER
IN CRYSTAL GROWTH

Prepared By: Samuel Sang-Moo Han
Academic Rank: Associate Professor
University and Department: Tennessee Tech University
Department of Mech. Eng.
NASA/MSFC:
Laboratory: Structures and Dynamics
Division: Earth and Atmospheric
Science
Branch: Fluid Dynamics
NASA Colleague: Charles F. Schafer
Cheryl Morroni
Date: August 14, 1987
Contract No: The University of Alabama
in Huntsville
NGT-01-002-021

ABSTRACT

A numerical analysis of transient heat and solute transport across a rectangular cavity is performed. Five nonlinear partial differential equations which govern the conservation of mass, momentum, energy and solute concentration related to crystal growth in solution, are simultaneously integrated by a numerical method based on the SIMPLE algorithm.

Numerical results showed that the flow, temperature and solute fields are dependent on thermal and solutal Grashoff number, Prandtl number, Schmidt number and aspect ratio. The average Nusselt and Sherwood numbers evaluated at the center of the cavity decrease markedly when the solutal buoyancy force acts in the opposite direction to the thermal buoyancy force. When the solutal and thermal buoyancy forces act in the same direction, however, Sherwood number increases significantly and yet Nusselt number decreases.

Overall effects of convection on the crystal growth are seen to be an enhancement of growth rate as expected but with highly non-uniform spatial growth variations.

ORIGINAL PAGE IS
OF POOR QUALITY

ACKNOWLEDGEMENT

I would like to thank Dr. Gerald Karr, Co-Director of NASA/ASEE MSFC program for extending me an invitation to participate in this program.

Dr. Charles Schafer deserves a special recognition for suggesting an interesting research topic and providing me with continuing guidance and encouragement. Ms. Cheryl Morroni and Dr. Ramachandran, distinguished members of microgravity working group, gave me strong encouragement and support.

There are many friends who made my stay at MSFC much easier and enjoyable through their hospitality: Drs. Nate Reynolds, Yemo Fashola, Y. S. Chen, Rand Decker and Tim Miller. John Parker, Karen Parker and Alan Johnston helped me with computer use and graphics. I thank them for their help.

My family had a very rough time living in a make-shift arrangement throughout ten weeks. They deserve more than thanks from me. They deserve a vacation. Thanks, Kee, Michael and Alex. You are the best bunch!

NOMANCLATURE

a	=H/L=aspect ratio of the cavity
A, B	species A and B
Cv, Cp	specific heat at constant volume and constant pressure
D _{AB}	diffusion coefficient of A through B
E	internal energy, Eqn (3)
g	gravitational acceleration
Gr _T	= $g\beta\Delta T H^3 / \nu^2$ = thermal Grashof number
Gr _M	= $g\alpha_A \Delta W_A H^3 / \nu^2$ = solutal Grashof number
H	cavity height
L	cavity width
Le	= ν/D_{AB} = Lewis number
N	buoyancy ratio, Eqn (18)
Nu	Nusselt number, Eqn (10)
P	dynamic pressure
Pr	= ν/α = Prandtl number
Q _H	net energy flux, Eqn (11)
Q _M	net mass flux, Eqn (15)
S	source terms, Table 1
Sc	= ν/D_{AB} = Schmidt number
Sh	average Sherwood number, Eqn (14)
Ra _T	=Gr _T x Pr = thermal Rayleigh number
Ra _M	=Gr _M x Sc = solutal Rayleigh number
t	time
T	temperature
u, v	flow speed in x- and y-direction
u _o	= ν/H = residence velocity
x, y	horizontal and vertical coordinates
W _A	= ρ_A/ρ = mass fraction of species A

Greek Symbols

ρ	= $\rho_A + \rho_B$ = density
μ	dynamic viscosity
ν	kinematic viscosity
α	= $K/\rho c_p$ = thermal diffusivity
K	thermal conductivity
$\delta x_i, \delta y_j$	control volume size in x and y
δt	time step
δ_T, δ_c	thermal and concentration boundary layer thickness
α_A	solutal expansion coefficient
β	thermal expansion coefficient
ΔT	= $T_H - T_C$ = temperature difference
ΔW_A	= $W_{A_H} - W_{A_C}$ = mass fraction difference

Super Scripts

~	nondimensional quantities
o	initial conditions

I. INTRODUCTION

OE POOR QUALITY

Single crystals are solid with the most uniform atomic structure that can be attained. This uniformity is the basis for a wide range of technological applications of single crystals. The most important feature of crystal is that it allows the transmission of acoustic, electromagnetic and charged particle with a minimal scattering. In particular, this transparency can be selectively modified by the controlled addition of impurities (dopants) to produce semi-conductor materials.[1]

Crystals are made from carefully controlled phase changes that involve solidification of a high temperature melt (melt growth), growth from low temperature mixture (solution growth) and condensation of a vapor (vapor growth). In all of these methods, the the nutrient materials are in either liquid or vapor phase. The physical transport mechanism at the interface between a nutrient fluid and the solid surface of growing crystal is controlled by mass diffusion. The solute gradient at the interface is , however, critically dependent upon the solute and thermal distribution of the nutrient fluid far away from the interface. This far-field flow behavior is controlled by the convection which is produced by various physical mechanism. Convection can be generated by the density gradients in a gravitational field (natural convection), or by an externally applied pressure (forced convection) or by both (mixed convection). In a low gravity environment, surface tension driven convection can be important when the nutrient fluid is allowed to have a free surface. Thus, in general, the growth of crystals is a coupled process of heat and mass transport, fluid flow , phase transformation and chemical reactions.

Even though the technology of crystal growth is well grounded in physical chemistry and materials science, the treatment of transport processes sometimes have been rudimentary and qualitative. To improve the quality of crystals, it is apparent that the flow characteristics at the growing interface must be understood so that one can control whatever influences the convection might have on the quality of crystals. Significant attempts have been made in recent years by fluid dynamicists to understand the complex interactions among various transport and physical processes in crystal growth. [1,2,3,4]

II. OBJECTIVES OF THE PRESENT RESEARCH

Much of the earlier works on the study of convection in crystal growth were based on the premise that convection is deleterious and therefore should be kept minimum at all cost. Materials processing in a space environment would provide a low gravity environment which will reduce buoyancy induced natural convection significantly. It is not likely however to create a completely acceleration free environment. A space station in which materials processing would occur is subject to microgravity due to near earth orbit and viscous drag force. Diffusion

processes in crystal growth are usually extremely slow and natural convection created by transient microgravity could be in the same order of magnitude. Surface tension driven natural convection, which is usually insignificant in terrestrial conditions, becomes very important in low gravity environment when the crystals are made by a containerless process.[2]

The purpose of the present research is to initiate a development of a numerical model which can be used to simulate crystal growth in realistic space environments. The thermal and solutal fields encountered in crystal growth from solution are, in general, three-dimensional and time-dependent. Transport properties, such as thermal diffusivity, mass diffusivity and fluid viscosity are general functions of solute concentration and fluid temperature of the mixture. Solidification processes usually involve liberation of latent heat at the interface. Also, rate of solidification depends on segregation (distribution) coefficient, which in turn depends on fluid temperature. A full scale three-dimensional model which accounts for all these physical conditions is not warranted until sufficient analyses of simplified two-dimensional situations are performed.

As a first step, a two-dimensional, time-dependent natural convection driven by both thermal and solutal buoyancy forces is selected in this research. Even though this physical model is far simpler than the actual processes, it should provide insights into the complex interactions between thermal and solutal convections encountered in crystal growth. Detailed descriptions on the physical model and appropriate equations are presented in section III. Numerical results are presented in section IV followed by conclusions and recommendations in section V.

III. FORMULATIONS

Two-dimensional thermal and solutal convection across a rectangular cavity is depicted in Figure 1. The vertical walls are maintained at isothermal and uniform mass-fraction of component A and the horizontal walls are assumed to be adiabatic and impermeable to mass diffusion. The fluid in the cavity is made of two components of liquid (say, A and B) with different molecular weights. Heat transfer occurs from the high temperature surface (left wall) to the low temperature surface (right wall). Mass transfer of species A also occurs from the left surface where the mass concentration of A is higher than at the right surface. It is assumed that all surfaces are impermeable to species B. One might consider species A to be a dopant in melt growth or crystal material in vapor or solution growth. Relative location of higher temperature wall and higher concentration surface is immaterial.

Thermal conduction occurs from the hot surface to the fluid and the temperature of the fluid increases over its initial value. Since the volume of most fluid expands as increasing

temperature, density of the fluid becomes less than its surrounding fluid. Lighter fluid elements rise up when the gravity acts along downward. This buoyancy force sets the convective flow motion within the cavity. Buoyancy force will act along the downward direction next to the cold surface at the right. Unless the initial temperature difference between the walls and fluid is large, the amount of heat transfer is small and the density change is almost negligible. This is known as the Boussinesq approximation. Mass diffusion from the left surface to the fluid will have similar effects on the flow field. Suppose species A has higher molecular weight than species B. Then diffusion of species A into the fluid will increase the density of the mixture and the solutal buoyancy force will act downward near the left wall. If the molecular weight of species A is lower than B, the solutal buoyancy force will be in the opposite direction. Since the mass diffusion through liquid is extremely slow, Boussinesq approximation can be invoked for mass transfer as well.

Governing Equations

The governing equations for the conservation of mass, momentum, energy and species A can be expressed by a generalized transport equation of the form

$$\frac{\partial \rho \phi}{\partial t} + \frac{\partial}{\partial x} \left[\rho u \phi - \Gamma \frac{\partial \phi}{\partial x} \right] + \frac{\partial}{\partial y} \left[\rho v \phi - \Gamma \frac{\partial \phi}{\partial y} \right] = S. \quad (1)$$

Table 1 contains appropriate expressions for ϕ , Γ and S for each equations.

Buoyancy forces due to thermal and solutal convections are included in the vertical direction momentum equation. All transport coefficients are assumed to be constants. No latent heat liberation is considered. The pressure appearing in the momentum equation represents only dynamic pressure. Static pressure is eliminated by using the density variation given by the Boussinesq approximation, i. e.,

$$\rho = \rho^0 [1 - \alpha_A (w_A - w_A^0) - \beta (T - T^0)]. \quad (2)$$

It is assumed that the mass concentration of species A of the liquid at the right vertical wall is equal to the mass concentration of species A at the solid. This assumption amounts to having a unit segregation coefficient at the growing surface. It is also assumed that the interfacial mass flux of species A at the vertical walls is negligible. (Interfacial mass flux can be calculated at these walls and the mass averaged flow velocities in the horizontal direction should be imposed at these walls for a more accurate boundary treatment.) Internal energy of the fluid is given by

$$E = C_v (T - T^0). \quad (3)$$

ORIGINAL PAGE IS
OF POOR QUALITY

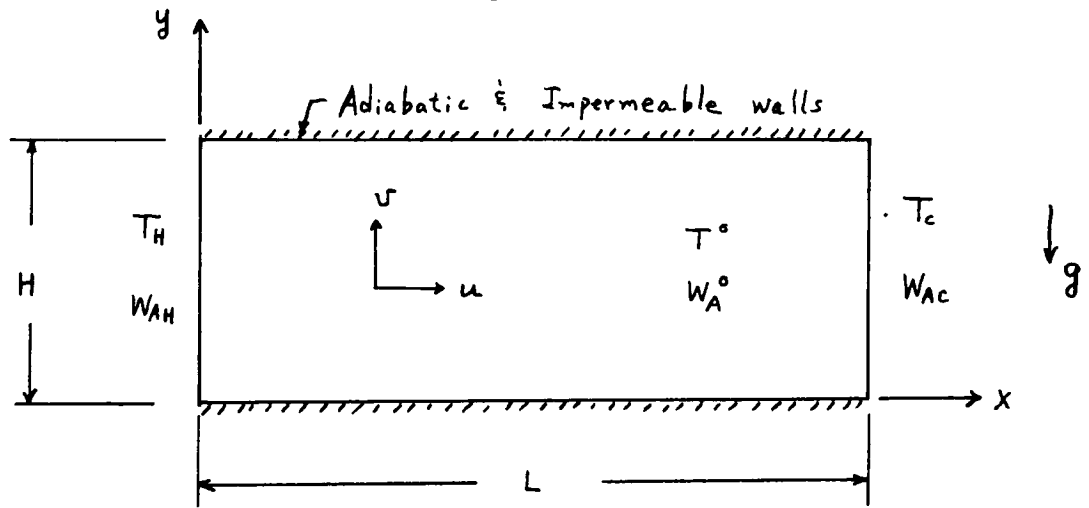


Figure 1. Geometry of the cavity

Table 1. Components of governing equations

	ϕ	Γ	S
Mass	1	0	0
X-momentum	u	μ	$-\frac{\partial p}{\partial x}$
y-momentum	v	μ	$-\frac{\partial p}{\partial y} + \rho g \beta (T - T^0) + \rho g \alpha_A (W_A - W_A^0)$
Energy	E	k/c_v	0
Concentration (Mass)	W_A	ρD_{AB}	0

Initial and Boundary Conditions

Initial and boundary conditions depend on the physical problems under consideration. Two types of initial conditions are considered; one corresponds to a static equilibrium condition and the other corresponds to a steady-state thermally driven natural convection. For the static initial conditions

$$\begin{aligned}
 u(x, y, t=0) &= v(x, y, t=0) = 0 \\
 \rho(x, y, t=0) &= \rho^0 \\
 T(x, y, t=0) &= T^0 \\
 W_A(x, y, t=0) &= W_A^0
 \end{aligned}
 \tag{4}$$

Boundary conditions are fixed for all numerical results reported in this paper. They are

$$\begin{aligned}
 T(x=0, y, t) &= T_H, \quad T(x=L, y, t) = T_C \\
 W_A(x=0, y, t) &= W_{AH}, \quad W_A(x=L, y, t) = W_{Ac} \\
 \left. \frac{\partial T}{\partial y} \right|_{x, y=0, t} &= \left. \frac{\partial T}{\partial y} \right|_{x, y=H, t} = \left. \frac{\partial W_A}{\partial y} \right|_{x, y=0, t} = \left. \frac{\partial W_A}{\partial y} \right|_{x, y=H, t} = 0
 \end{aligned}
 \tag{5}$$

Nondimensional Parameters

The present numerical method utilizes primitive variables in dimensional forms. It is convenient, however, to introduce appropriate flow characteristics into the governing equations to obtain important nondimensional parameters which govern the flow. Numerical and experimental data presented in nondimensional parameters are universal and can be used to infer other similar problems with different fluid properties and physical geometries.

Nondimensional variables are defined by

$$\begin{aligned}
 \tilde{x} &= \frac{x}{H} ; \quad \tilde{y} = \frac{y}{H} ; \quad \tilde{t} = \frac{t}{H/u_0} ; \quad \tilde{u} = \frac{u}{u_0} \\
 \tilde{v} &= \frac{v}{u_0} ; \quad \tilde{T} = \frac{T - T^0}{\Delta T} ; \quad \tilde{W}_A = \frac{W_A - W_A^0}{\Delta W_A}
 \end{aligned}
 \tag{6}$$

Introducing these nondimensional variables into the governing

equations (1), it can be readily shown that nondimensional equations contain five nondimensional parameters. They are; aspect ratio (a), thermal Grashoff number (Gr), solutal Grashoff number (Gr_s), Prandtl number (Pr), and Schmidt number (Sc). Numerical results will be presented in terms of nondimensional quantities.

VI. ANALYSIS

Numerical Method

The numerical method used for the present study is a finite volume method based on the SIMPLE algorithm.[5] Since a detailed description on the essence of SIMPLE can be found in a reference [5], it will not be discussed in this report.

The SIMPLE method, in principle, can be applied to both high speed flow as well as low speed flow by using a proper equation of state and including the density variations due to the pressure change. These modifications were added to the original SIMPLE method and the revised method were successfully applied to a transient acoustic wave propagation in a water hammer [6] and a transient natural convection in a square cavity [7].

Physical and Numerical Parameters

Physical and numerical parameters used for the present study are listed in Table 2. Physical properties are selected only to give representative thermal and solutal Grashof numbers, Prandtl and Schmidt numbers encountered in solution growth under terrestrial conditions. Thus these values may not represent any actual crystal growth environment. Numerical parameters are selected (by trial and error) such that either the solution approaches to the true solution (if exists) or converges to steady or quasi-steady solution within a reasonable computing time.

Numerical Results

Four different cases are simulated to investigate the effects of thermal and solutal convections and their interactions.

CASE 1: Thermal convection : Nondimensional parameters used for this case are

$$\begin{aligned} Gr_T &= 9 \times 10^5 ; Gr_M = 0 ; Pr = 7.07 ; a = 0.53 \\ Ra_T &= 6.36 \times 10^6 \end{aligned} \quad (7)$$

This case is studied first to check the accuracy of the numerical code developed. Thermally driven natural convection in

rectangular geometries are extensively studied and the present results can be easily checked against existing data.

Numerical accuracy and computational economy depend on the choice of computational mesh arrangement. Since the driving force for the present convection comes from the vertical walls. The resulting buoyancy driven convection will form thermal and momentum boundary layers. It is therefore necessary to have fine grids near the vertical walls. Invoking scale analysis for the boundary layer regime [8], the thermal boundary layer thickness is

$$\delta_T \sim H Ra_T^{-1/4} \approx 2.07 \times 10^{-3} \text{ m.} \quad (8)$$

The mesh size at the vertical walls therefore should be small enough that at least one computational mesh should be placed within this boundary layer. The mesh arrangement along the x-direction is given by

$$\delta x_{i+1} = \delta x_i (1 + \Delta x_{\%T}) \quad (9)$$

, where δx_i is the first mesh size and $\Delta x_{\%T}$ is the percent increment. The mesh arrangement near the horizontal walls need not be as small walls since the horizontal walls are adiabatic and the momentum boundary layer is thicker than the thermal boundary layer ($Pr > 1.0$). Grid expansion along the y-direction is similar to x-direction. Number of trial runs were made before settling to the mesh arrangement as shown in Figure 4a. Total 26 (X-direction) by 20 (Y-direction) meshes were used in all subsequent computations. (Actually, the first mesh size near the vertical walls are much larger than the thermal boundary layer thickness. However, solutal boundary layer thickness, discussed later, dictates this size.)

Figure 2 shows transient behavior of rate of energy transfer across the cavity evaluated at the center of the cavity. Nusselt number is defined by

$$Nu_L = \frac{Q_H}{H \frac{k}{L} \Delta T} \quad (10)$$

where Q_H represents the total energy flux given by

$$Q_H = \int_0^H \left[\rho u c_p (T - T^0) - k \frac{\partial T}{\partial x} \right]_{x=\frac{L}{2}} dy. \quad (11)$$

Table 2. Physical and Numerical Parameters

Parameters	Values	Dimension
C_v, C_p	1.0	$m^2/s^2 \cdot K$
μ	$8.55E-3$	$kg/m \cdot s$
ρ^0	1000	kg/m^3
g	9.81	m/s^2
β	$6.0E-4$	K^{-1}
α_A	+0.27E -0.27E	dimensionless
K	5.0	$kg \cdot m / K \cdot s^3$
T^0	300	K
W_A^0	0.9	dimensionless
ΔT	10	K
ΔW_A	0.2	dimensionless
D_{AB}	$4.0E-9$	m^2/s
H	0.10384	m
L	0.19526	m
$\delta x_i, \delta y_i$	0.0005 - 0.028	m
δt	0.1 - 5.0	s
ϵ	$1.0E-3$	dimensionless

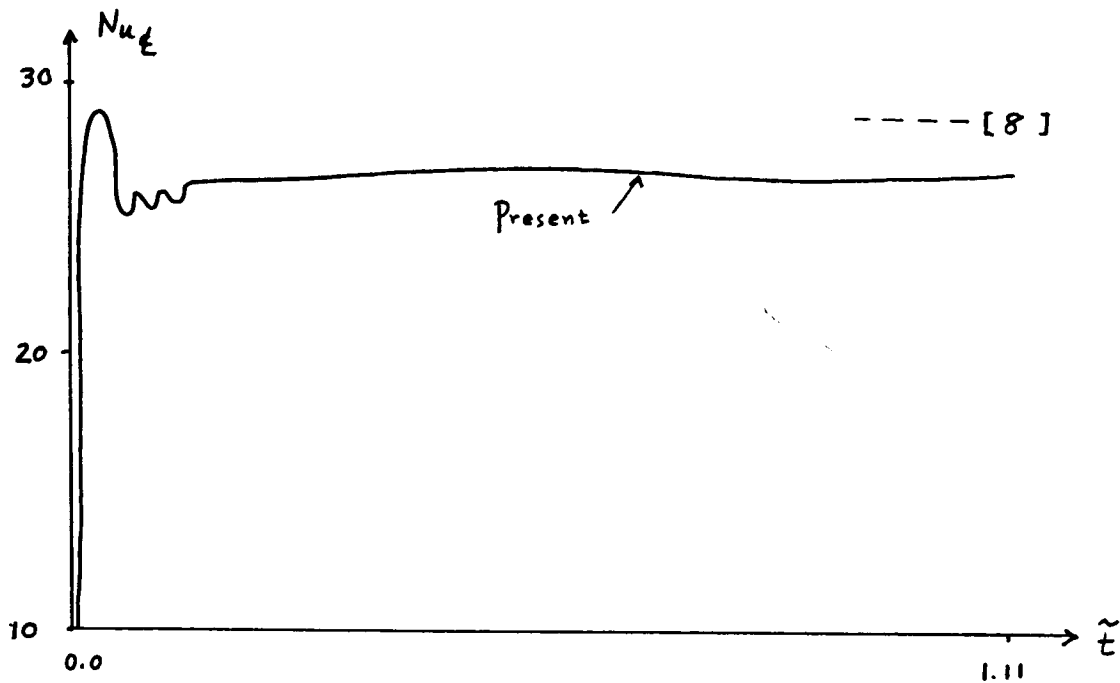


Figure 2. Transient Nusselt Number (Case 1)

Nusselt number increases rapidly as the hot and cold fluid intrude the top and bottom portions of the cavity. Energy transfer is at the maximum when the convection velocity reaches the maximum at this early stage of transient convection. Numerical solution exhibits oscillatory horizontal flow speed. These oscillations are mainly responsible the oscillatory Nusselt number. Oscillatory energy transfer across a square cavity was theoretically predicted by Patterson and Imberger [9] and was numerically confirmed. [7,9] Oscillation periods and amplitudes for the present case ($a=0.53$) are different from those for $a=1.0$ reported in ref[7,9].

Steady-state Nusselt number computed by the present simulation is about 27. Bejan [8] obtained the analytical solutions for the boundary layer regime with $Pr > 1$. Figure 3 shows the average Nusselt number obtained by his solutions. Using his results, the average Nusselt number for the present case is about 29, which is in reasonable agreement with the computed value.

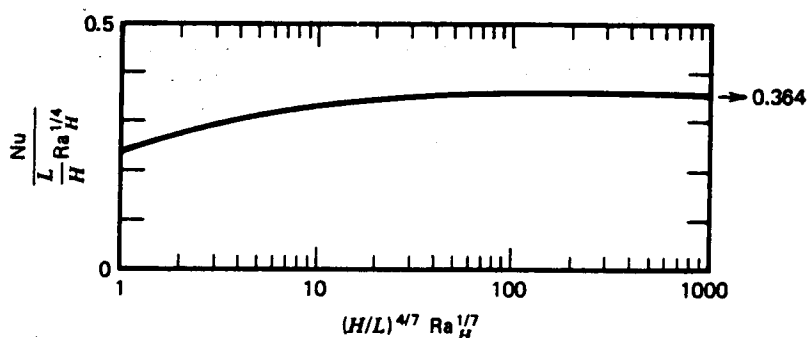


Figure 3. Nusselt number correlations [8]

Figure 4 shows the global view of steady-state flow and temperature fields for Case 1. Very thin thermal and momentum boundary layers are developed at the vertical walls. Temperature in the core regions are highly stratified and isotherms are almost parallel. Most of the fluid in the core is relatively stagnant.

Figure 5 shows the temperature and velocity profiles at two selected spatial locations in the cavity. Figure 5a shows the vertical velocity and fluid temperature at a horizontal plane located at the mid-height of the cavity. Thermal boundary layer is located within the momentum boundary layer and the over-all boundary layer thickness is in the order of % of the cavity width. Figure 5b shows the horizontal velocity and temperature of the fluid at the vertical plane located at the mid-width of the cavity. Magnitude of horizontal velocity and temperature distribution at this plane as shown in Figure 5b determines the energy transfer rate across the cavity. Note that the vertical velocity is order of magnitude higher than the horizontal velocity.

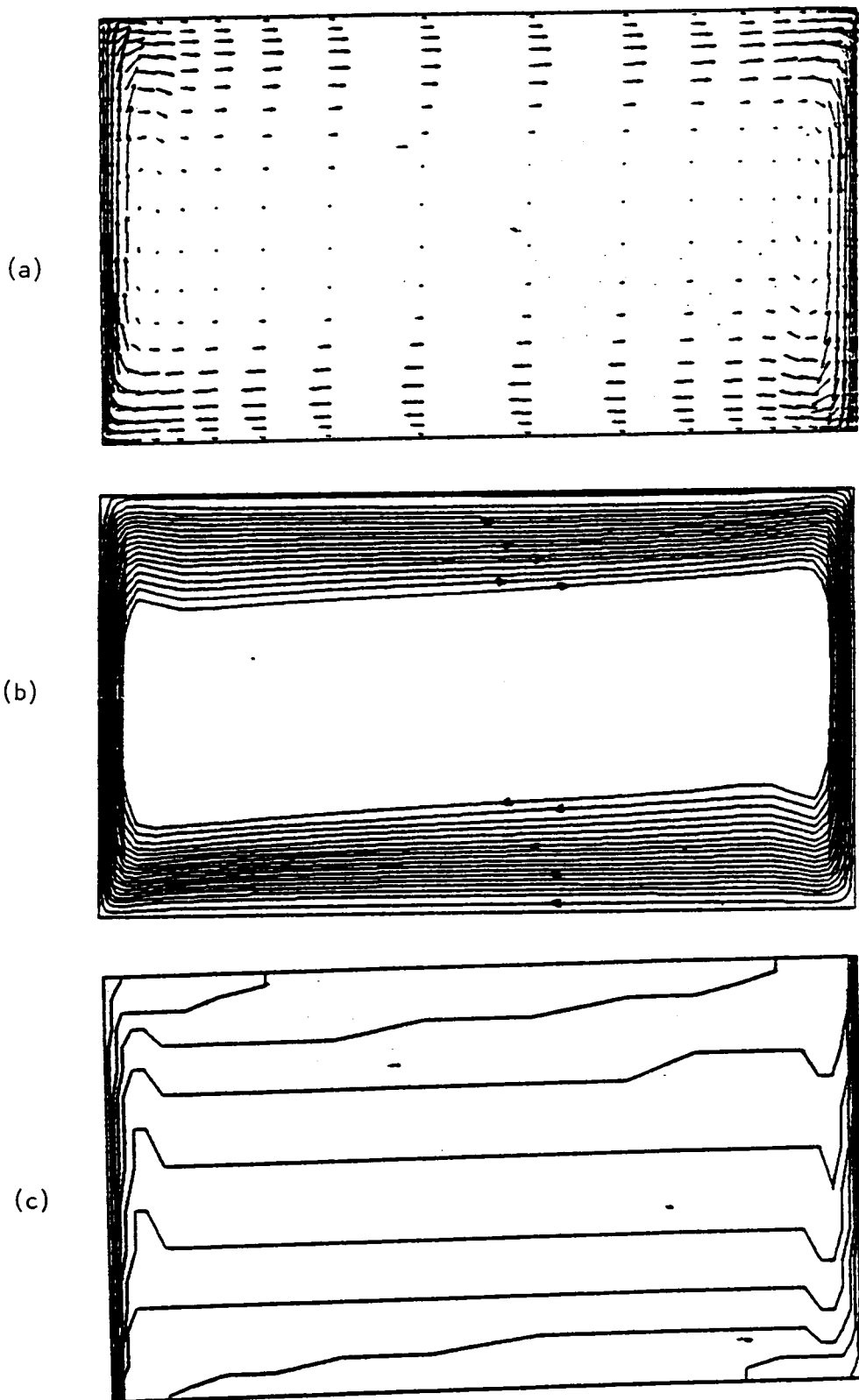


Figure 4. Steady-state velocity vector (a), stream lines (b) and isotherms (c) for Case 1

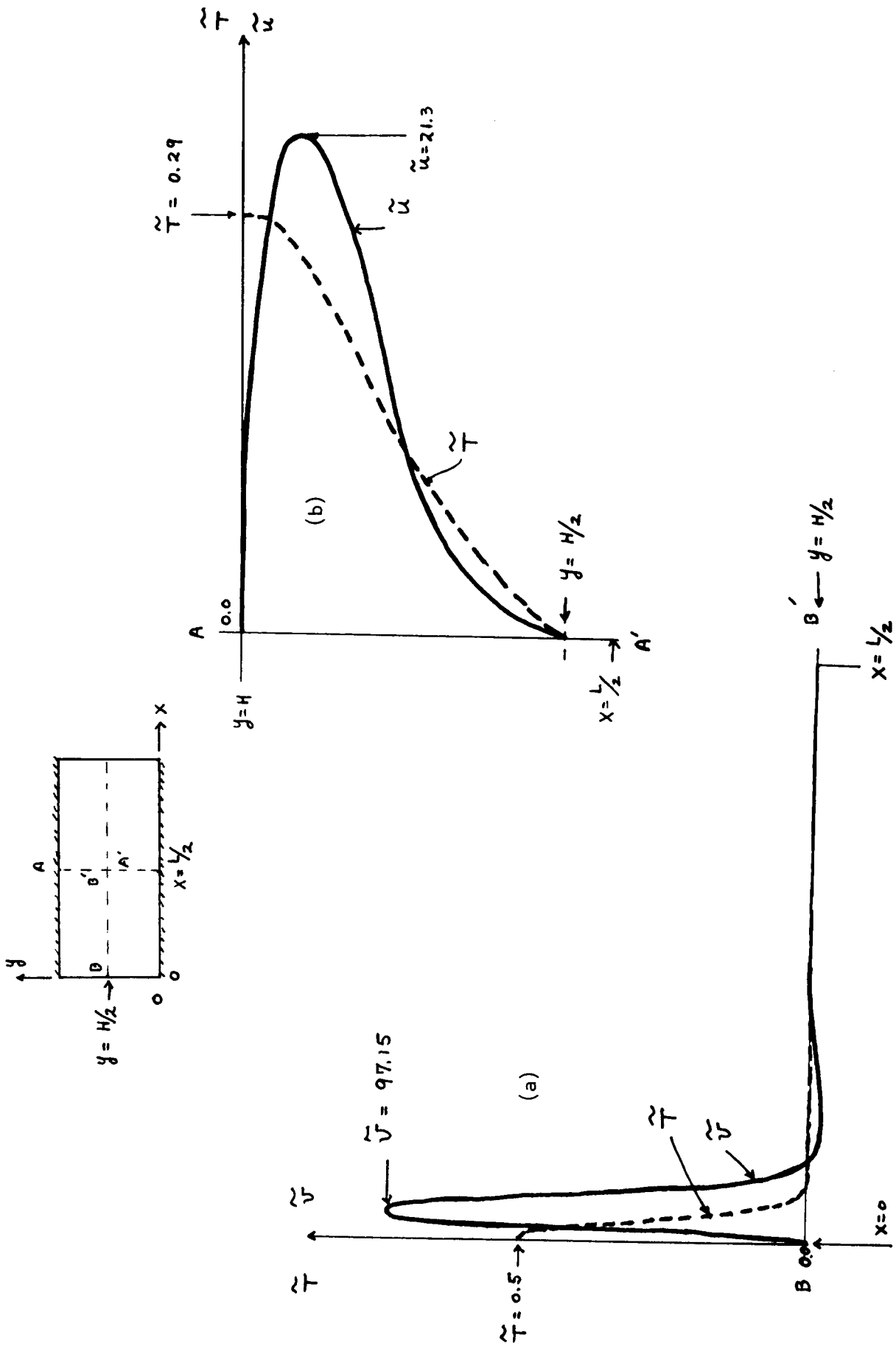


Figure 5. Velocity and temperature profiles at selected planes

CASE 2: Solutal convection: Nondimensional parameters used for this case are

$$Gr_M = -8.3 \times 10^6 ; Gr_T = 0 ; Sc = 2140 ; A = 0.53$$

$$Ra_M = 1.78 \times 10^{10} \quad (12)$$

Nondimensional solute concentration equation is identical to the nondimensional energy equation except the Schmidt number appears in place of the Prandtl number. By virtue of this analogy between equations, average mass transfer of species A across the cavity can be determined by using the Nusselt number correlations with simple replacement of nondimensional parameters such as

$$Pr \rightarrow Sc \quad Gr_T \rightarrow Gr_M \quad Nu \rightarrow Sh \quad (13)$$

Using the results of Nusselt number correlation as shown in Figure 3, the average steady-state Sherwood number corresponding to the given mass Rayleigh number is approximately 226.

Figure 6 shows the computed transient Sherwood number evaluated at the center of the cavity defined by

$$Sh_z = \frac{Q_M}{\rho D_{AB} \frac{H}{L} \Delta W_A} \quad (14)$$

where Q_M is the net mass transfer of species A at the center of the cavity and given by

$$Q_M = \int_0^H \left[\rho u (W_A - W_A^0) - \rho D_{AB} \frac{\partial W_A}{\partial x} \right]_{x=\frac{L}{2}} dy \quad (15)$$

Mass transfer increases sharply as the convection current reaches the center of the cavity and undergoes a weak oscillation before approaching the steady value of about 222. This is in excellent agreement with the analytical result.

Using the analogy, solutal boundary layer thickness can be computed as

$$\delta_c \sim H Ra_M^{-1/4} \approx 2.84 \times 10^{-4} \text{ m.} \quad (16)$$

This implies that the center of the control volume next to the vertical wall should be less than 2.84×10^{-4} m. The present grid system ($\delta x_1 = 0.0005$) does satisfy this requirement. When the grid size of the control volume next to the vertical walls was doubled ($\delta x_1 = 0.001$) the steady Sh number was 170 and when $\delta x_1 = 0.002$, $Sh = 97$.

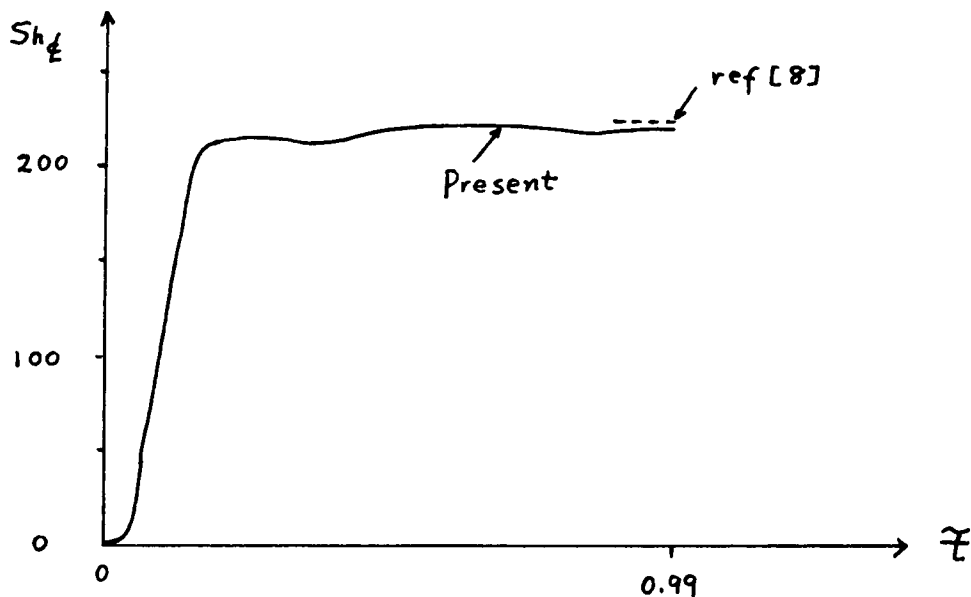


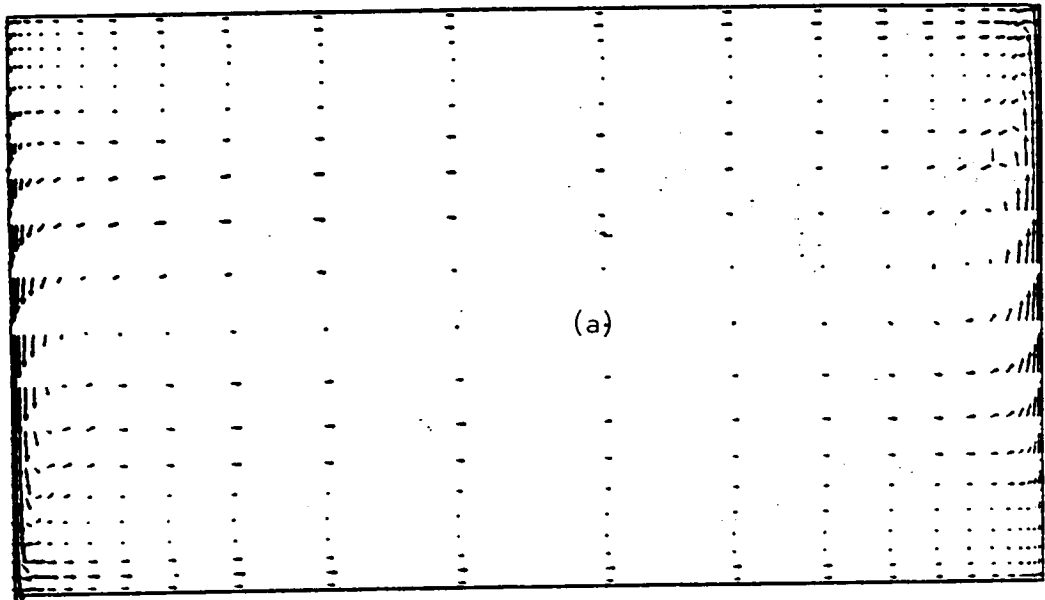
Figure 6. Transient Sherwood number variations (Case 2)

The amplitude and frequency of Sherwood number oscillations are much smaller than the Nusselt number oscillations as shown in Figure 2. This is due to extremely high Schmidt number (2140) used in Case 2 compared with a smaller Prandtl number (7.0) used in Case 1. Viscous damping is more pronounced in Case 2.

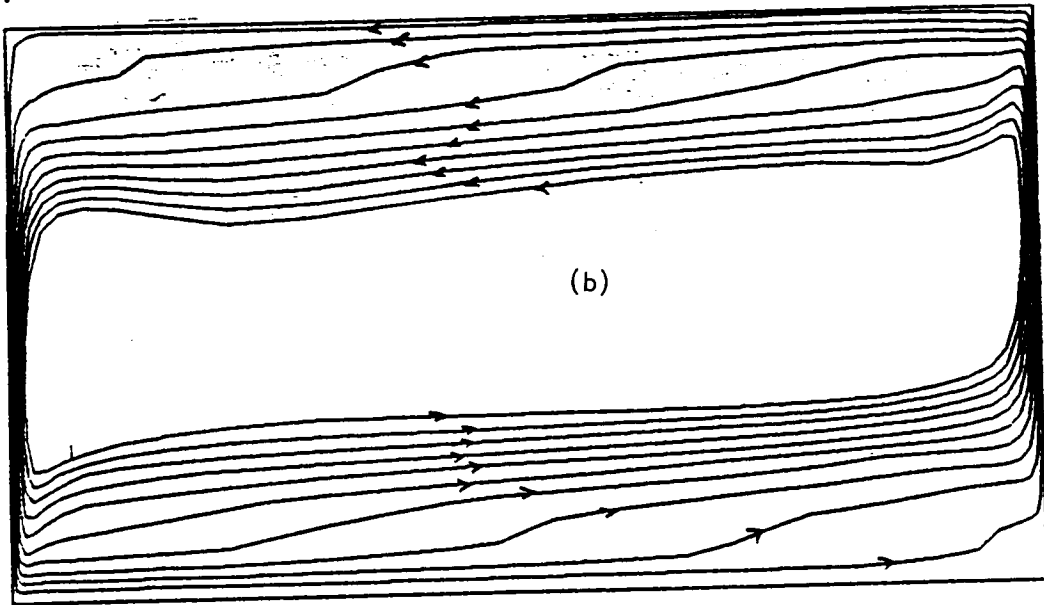
Figure 7 shows the steady-state flow, temperature and concentration field for Case 2. Note that the solutal buoyancy force acts along the negative y -direction near the left wall. The magnitude of convection is much smaller than the Case 1 and the momentum boundary layer thickness is much smaller than Case 1. Furthermore, solutal boundary layer on the vertical walls (Figure 7c) are confined within one computational cells along the vertical walls.

The most peculiar aspect of the flow field in Case 2 is two-distinct horizontal convection layers along the horizontal walls. There are relatively dead flow zones between these horizontal convection currents. Figure 8 shows these peculiarity more clearly. Figure 8a shows the vertical velocity and concentration profiles at a horizontal plane at the cavity mid-height. Figure 8b shows the horizontal velocity and concentration profiles at a vertical plane at the mid-width of the cavity. Horizontal velocity distributions have double humps. Mass transfer across the cavity is however mainly contributed by the convection current near the horizontal walls since the mass concentration remains mostly at the initial value around the second velocity maximum.

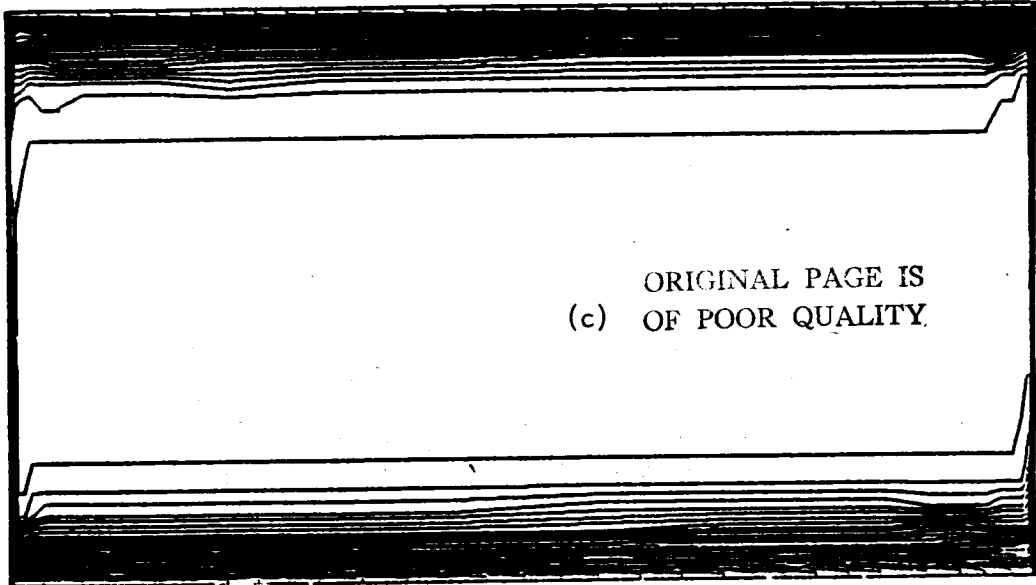
Layered convection could occur, for example, when a stable water (saturated with salt) is heated from the side wall. Heat transfer to water occurs from the wall by conduction. Heated



(a)



(b)



(c) ORIGINAL PAGE IS
OF POOR QUALITY.

Figure 7. Steady-state velocity vectors (a), stream lines (b) and iso-concentrations for Case 2

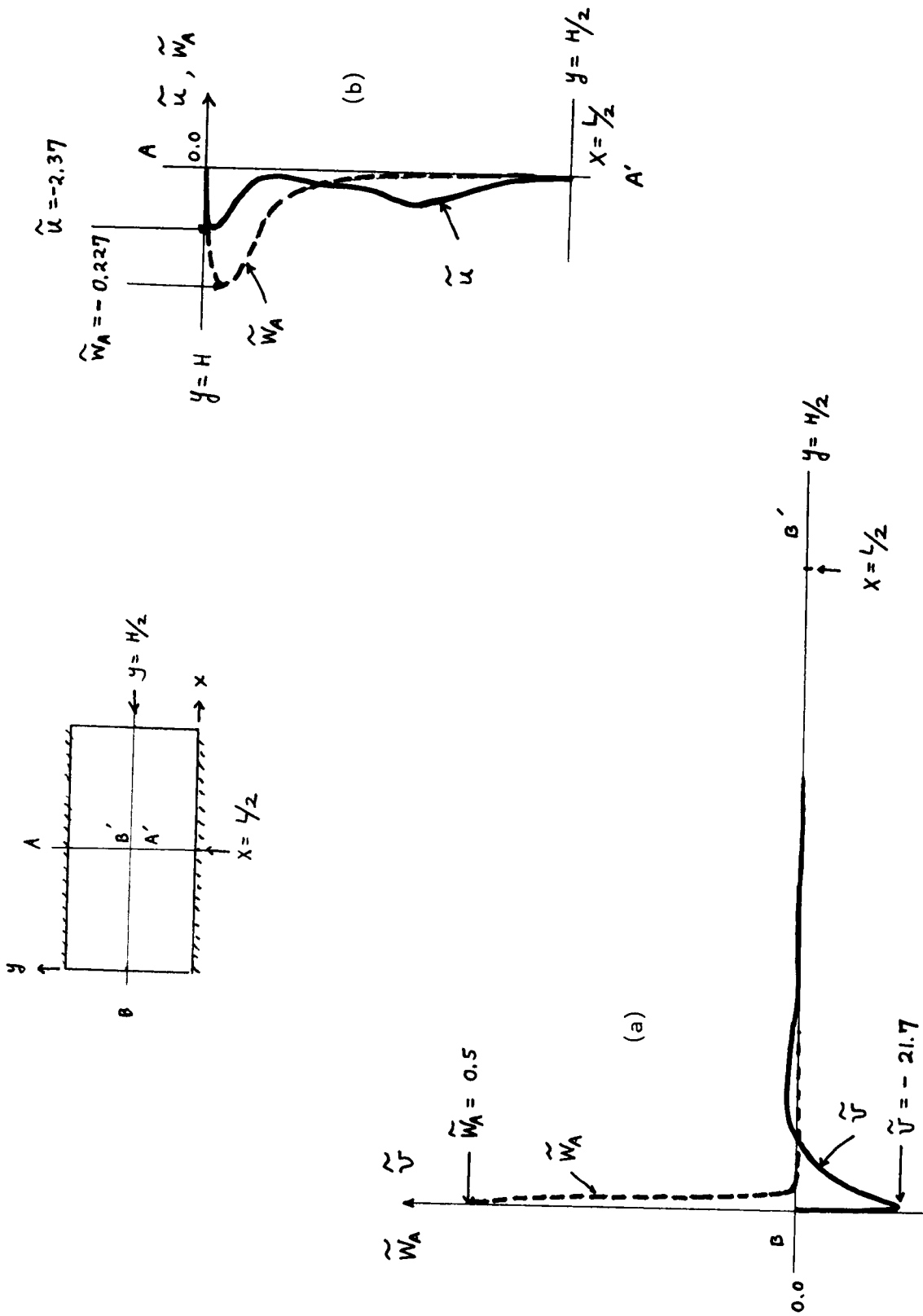


Figure 8. Velocity and mass concentration profiles at selected planes for Case 2

water expands and rises up to the level where its density matches the surrounding density and flows horizontally away from the hot wall. If the mass diffusivity of salt through water is equal to the thermal diffusivity, density change due to heat transfer and mass transfer can cancel each other. In this case, layered convection can not occur. Double-diffusive flow involves two distinct diffusion processes with different diffusion coefficients. The present results are somewhat similar to double-diffusive flow situation even though mass transfer is the only available diffusion mechanism. No satisfactory physical explanation can be offered at present moment to explain the layered convection in Case 2.

CASE 3. Opposing combined convection: In this case both thermal and solutal buoyancy effects are considered. The initial flow and temperature fields are those obtained in Case 1. Solutal buoyancy force acts in the opposite direction to the thermal buoyancy force. Nondimensional parameters are

$$\begin{aligned} Gr_T &= 9 \times 10^5 ; Gr_M = -8.3 \times 10^6 ; Pr = 7.07 ; Sc = 2140 ; \\ \alpha &= 0.53 ; Ra_T = 6.36 \times 10^6 ; Ra_M = 1.78 \times 10^{10} \end{aligned} \quad (17)$$

Two additional nondimensional parameters are defined in order to compare the thermal and solutal effects. They are Lewis number and the buoyancy ratio

$$Le = \frac{Sc}{Pr} = 302 ; N = \frac{\alpha_A \Delta W_A}{\beta \Delta T} = -9.27 \quad (18)$$

Figure 9 shows the average Nusselt and Sherwood number variations as a function of time for the combined convection. The

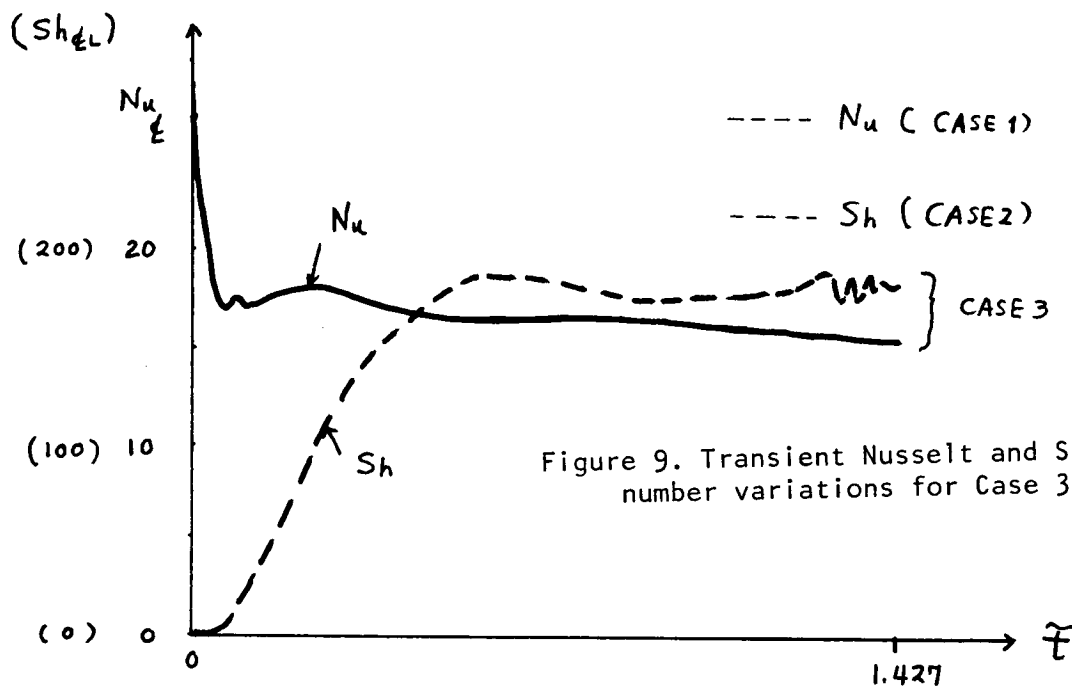


Figure 9. Transient Nusselt and Sherwood number variations for Case 3

ORIGINAL PAGE IS
OF POOR QUALITY

steady state Nusselt number for Case 1 and Sherwood number for Case 2 are also indicated for comparison. Due to the opposing buoyancy effects, energy and mass transfer rates are markedly dropped compared with a pure thermal and a pure solutal cases. Numerical solutions at the end of computations were not steady-state. Small fluctuations in Sherwood number are due to fluctuating velocity field. Qualitatively similar fluctuations were observed in experiments. [1]

Figure 10 shows the quasi-steady state flow, temperature and concentration fields at the end of computation. Two convection loops can be identified: a slow counter clockwise circulation near the solid walls due to solutal effects and a dominant clockwise circulation in the rest of the cavity. Overall flow characteristics are determined by the thermal effects because of high Lewis number. Temperature inversion (hotter fluid on top of cold) occurs at the lower left and top right corner of the cavity (Fig 10c) due to solutal effects.

CASE 4. Aiding combined convection: In this case, solutal buoyancy force and the thermal buoyancy force are acting along the same direction. Nondimensional parameters are identical to those of Case 3 except the change in sign for the buoyancy ratio. Initial conditions are again provided by Case 1.

Figure 11 shows the transient heat and mass transfer rate across the cavity for the aiding case in comparison with a pure thermal and a pure solutal cases. Numerical solutions, in particular the mass transfer rate, exhibit the mild fluctuations toward the end of computations as Case 3. Quasi-steady-state Sherwood number for the aiding case increased markedly over Case 2. However, Nusselt number is decreased below that of Case 1. This unexpected result is a consequence of thermal and solutal interactions, which is explained in a later section.

Figure 12 shows the quasi-steady velocity, temperature and concentration fields for Case 3. Over-all features are similar to case 1 (Figures 12a, 12b and 12c) and Case 2 (Figure 12d).

Thermal and Solutal Interactions

To analyse the thermal and solutal interactions more closely, detailed flow profiles at a horizontal plane located at the mid-height of the cavity are presented in Figure 13. It can be seen that opposing solutal buoyancy forces result in the negative vertical velocity near the left vertical wall and reduced vertical velocity compared with the pure thermal case. Temperature and concentration gradients at the left wall are also reduced compared with pure convection cases.

For the aiding case, vertical velocity is increased near the vertical wall due to the solutal buoyancy force as expected. However, vertical velocity is actually smaller than that of Case 1 in most of the remaining velocity boundary layer. Temperature gradient at the wall remains almost identical to Case 1. But

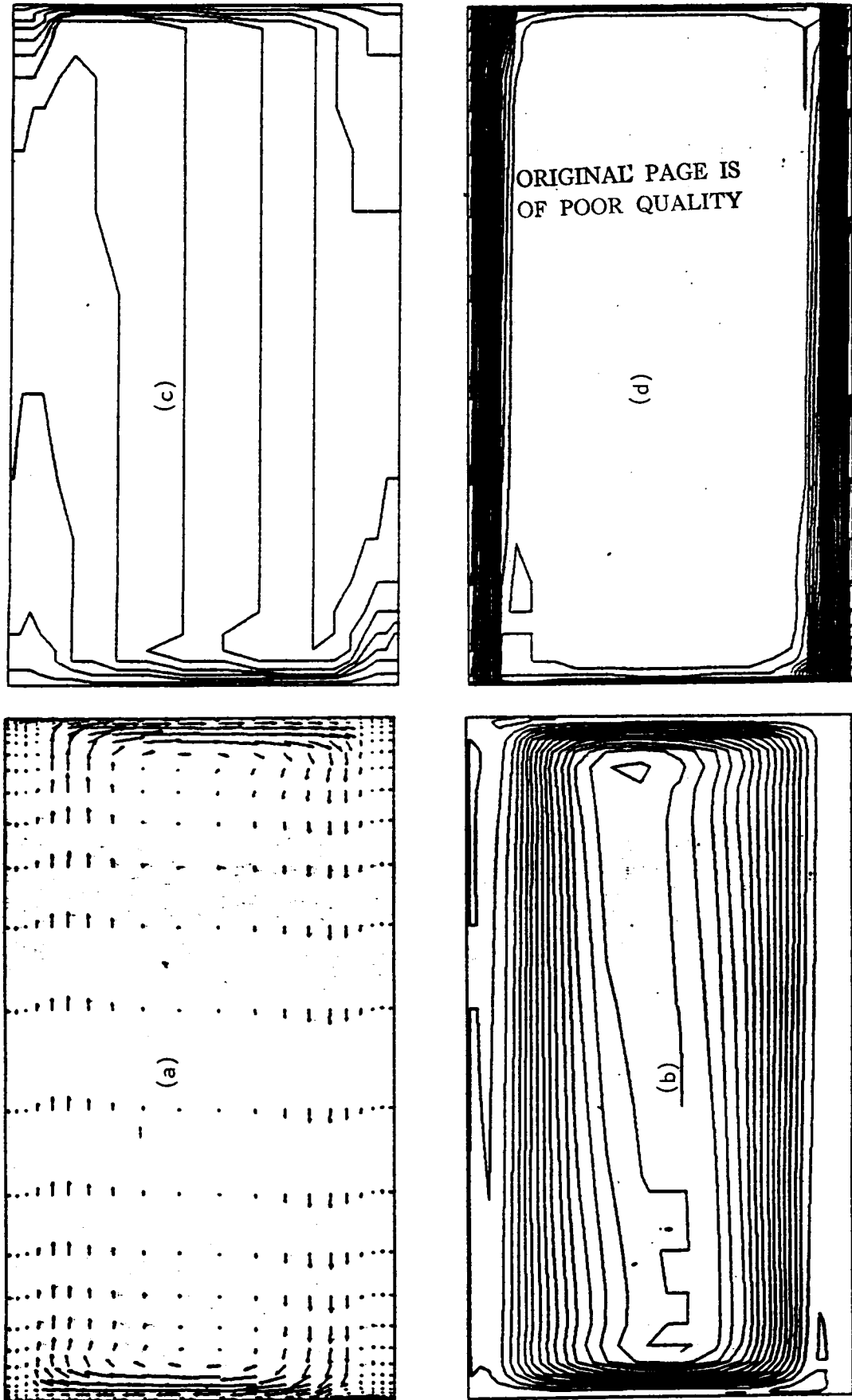


Figure 10. Quasi-steady-state velocity vectors (a), stream lines (b), iso-mass concentrations for Case 3 and

ORIGINAL PAGE IS
OF POOR QUALITY

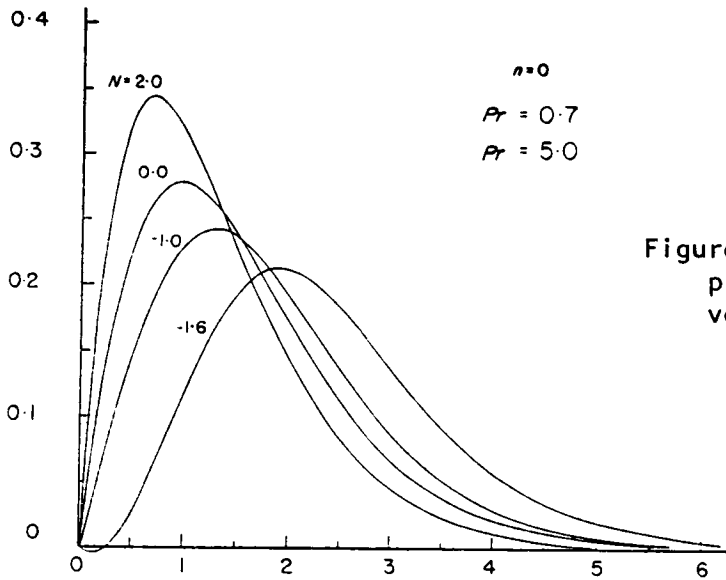


Figure 14. Vertical velocity profiles at an infinite vertical plane [11]

concentration gradient is much higher than that of Case 2 due to the increased vertical flow speed compared with Case 2. Consequently, Nusselt number for this aiding case is slightly lower than Case 1 but the Sherwood number is much higher than Case 2.

The velocity profiles shown in Figure 13a are similar to similarity solutions [11] over a vertical flat plate, except the aiding case. (Figure 14) Direct one to one comparison is not possible since two problems differ in geometry and nondimensional parameters.

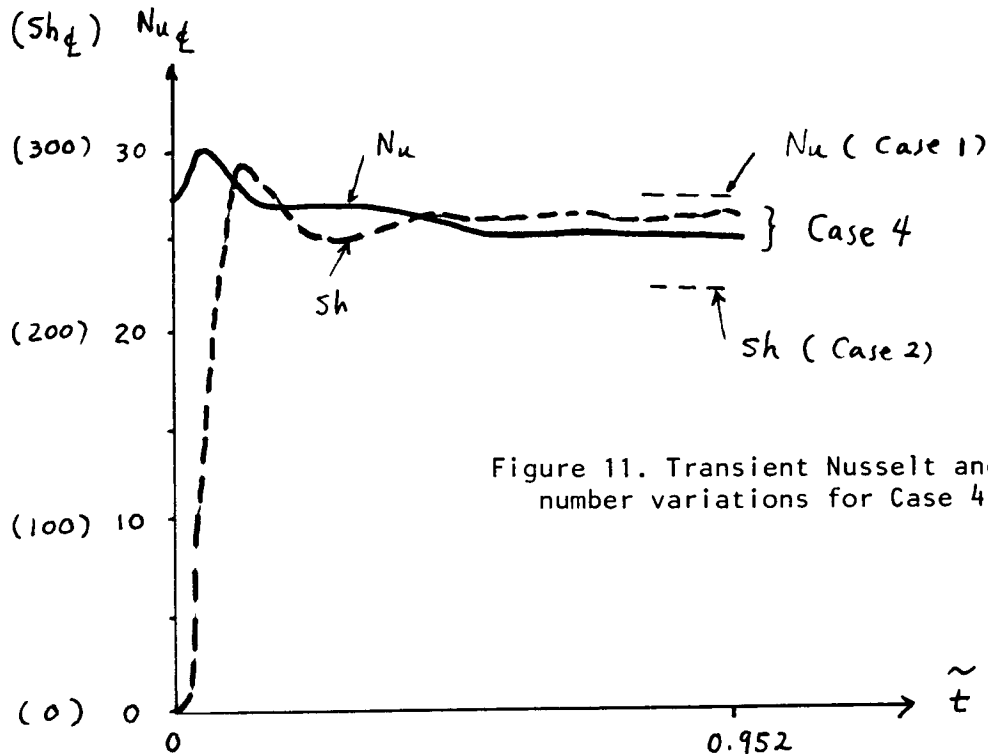


Figure 11. Transient Nusselt and Sherwood number variations for Case 4

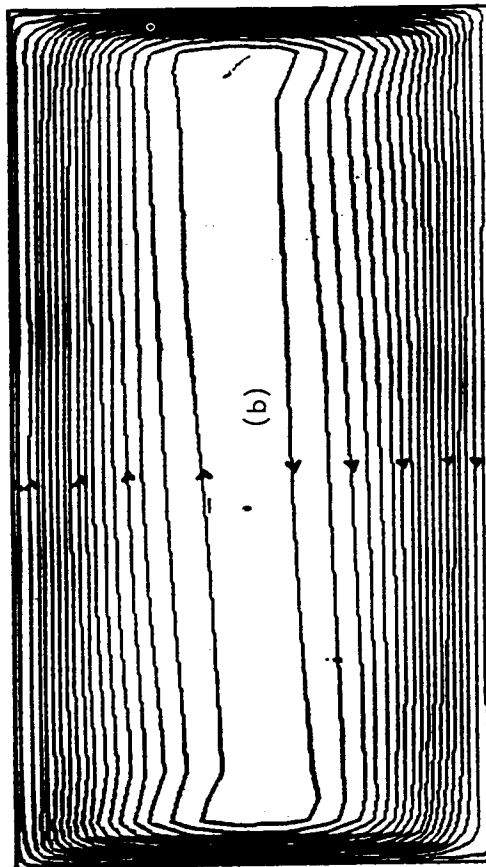
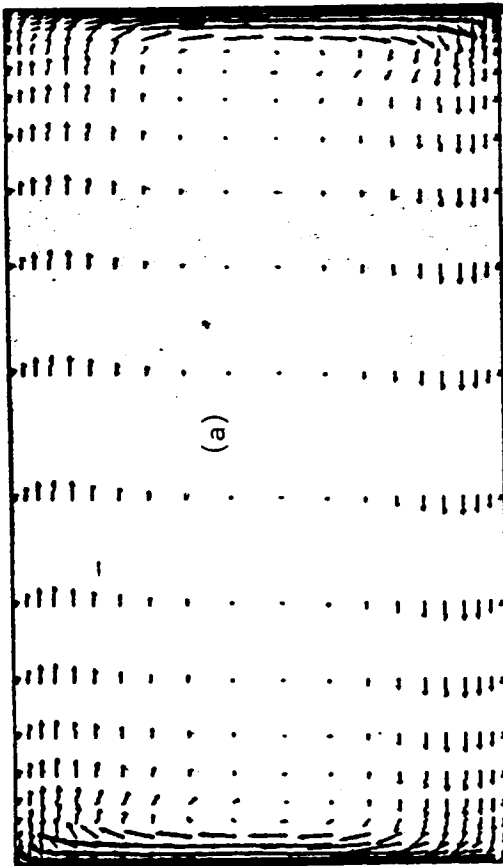
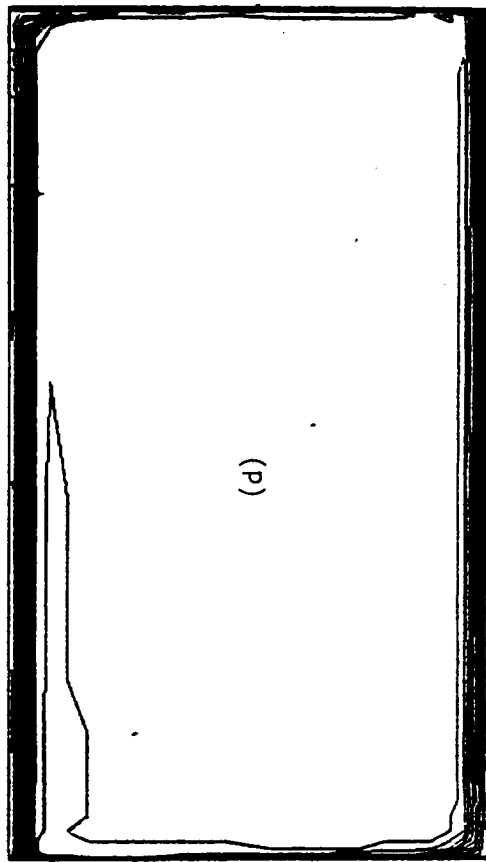
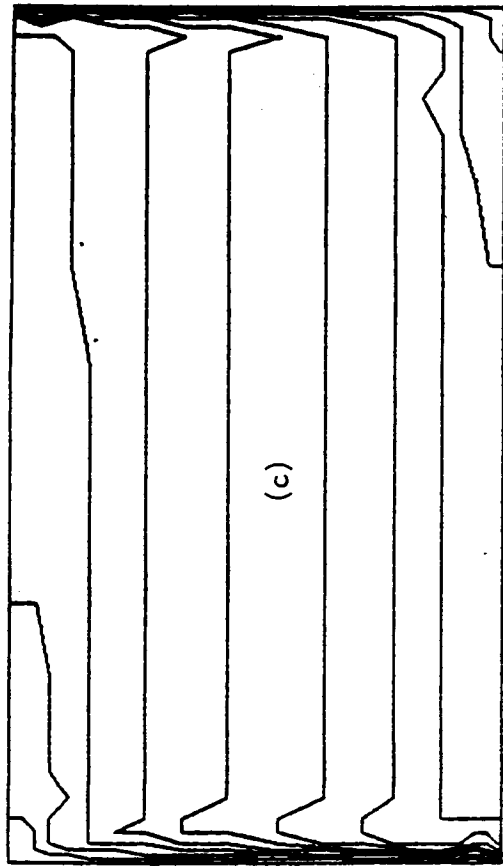


Figure 12. Quasi-steady-state velocity vectors (a), stream lines (b), isotherms (c) and iso-mass concentrations (d) for Case 4

ORIGINAL PAGE IS
OF POOR QUALITY

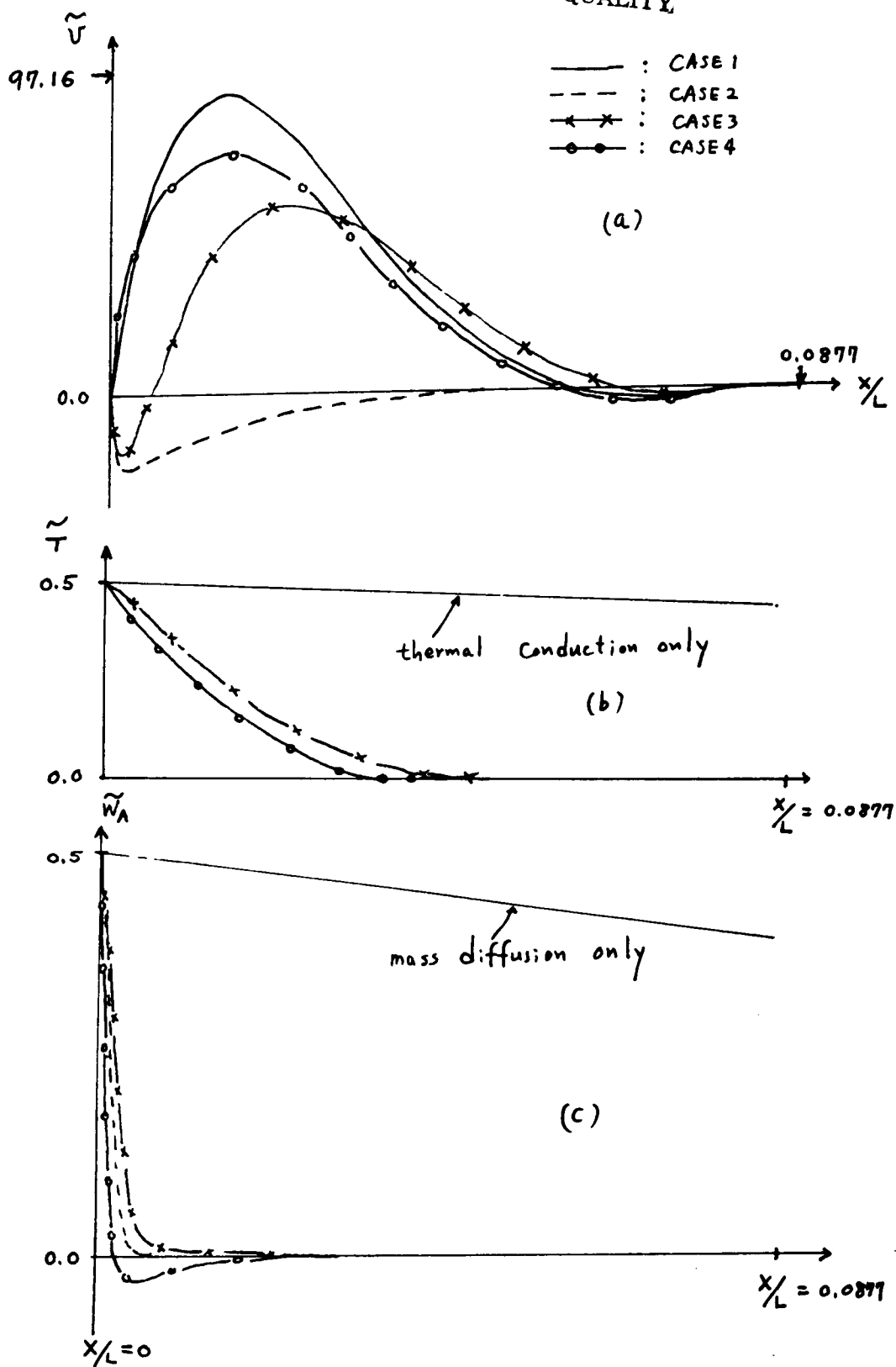


Figure 13. Vertical velocities (a), temperatures (b) and mass concentrations (c) distributions in boundary layers at the left vertical wall at the mid-height of the cavity

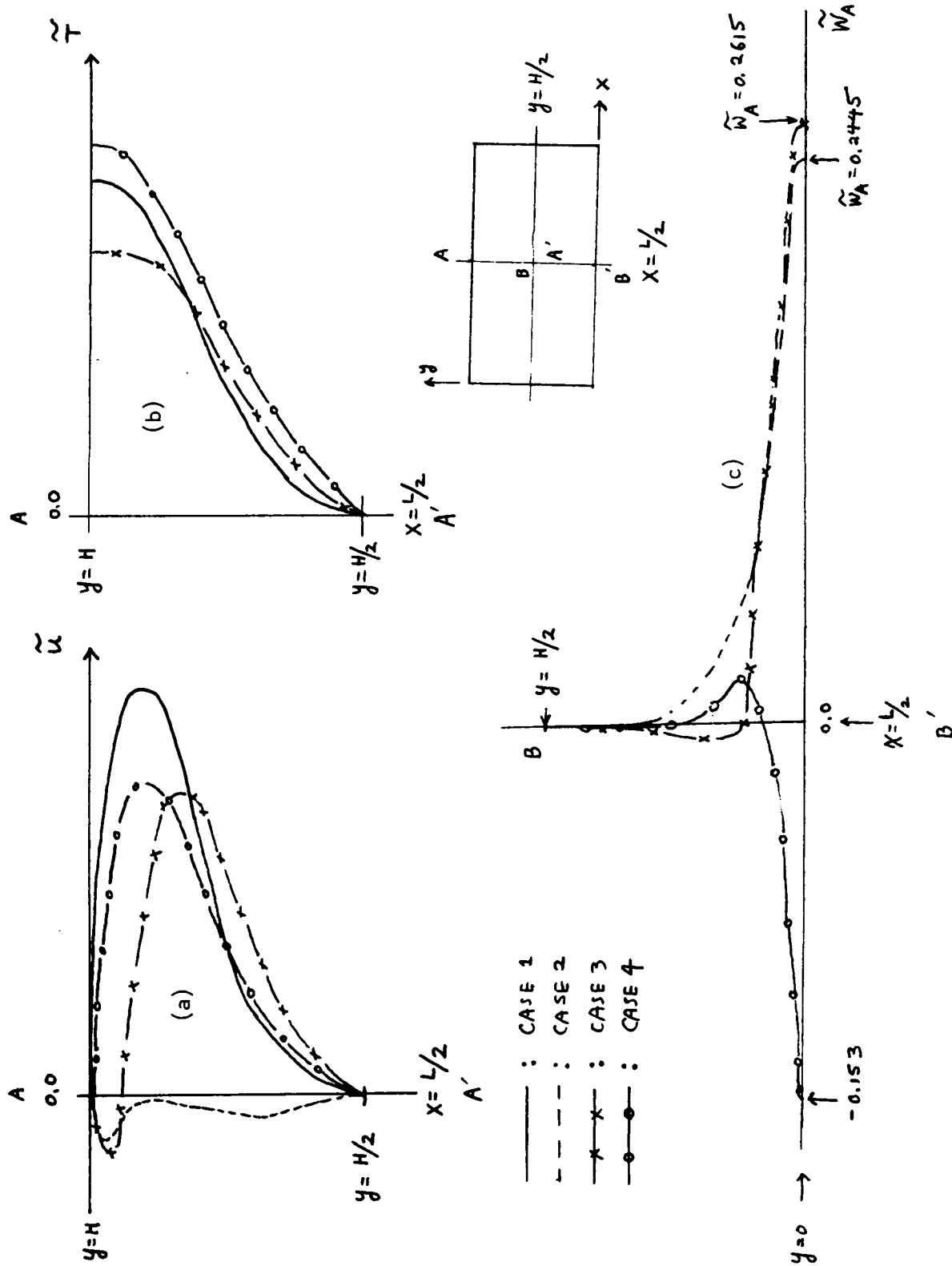


Figure 15. Horizontal velocity (a), temperature (b) and mass concentration distributions at a vertical plane located at the mid-width of the cavity

Figure 15 shows the horizontal velocity, temperature and concentration profiles at a vertical plane located at the mid-width of the cavity. These results again show that the mass and heat transfer across the cavity are strongly dependent on the interactions between the thermal and solutal convections and that opposing and aiding effects can have unexpected influences on the transport mechanisms.

Effects on Crystal Growth

Figure 16 shows the temperature and concentration at the center of the control volumes next to the right vertical wall, which might represent the growing surface of a crystal. Highly nonuniform temperature and concentration profiles there imply an uneven heat transfer and crystal growth rate. As expected, convection enhances the rate of crystal growth significantly over the pure diffusion cases but with detrimental effects on the crystal structure.

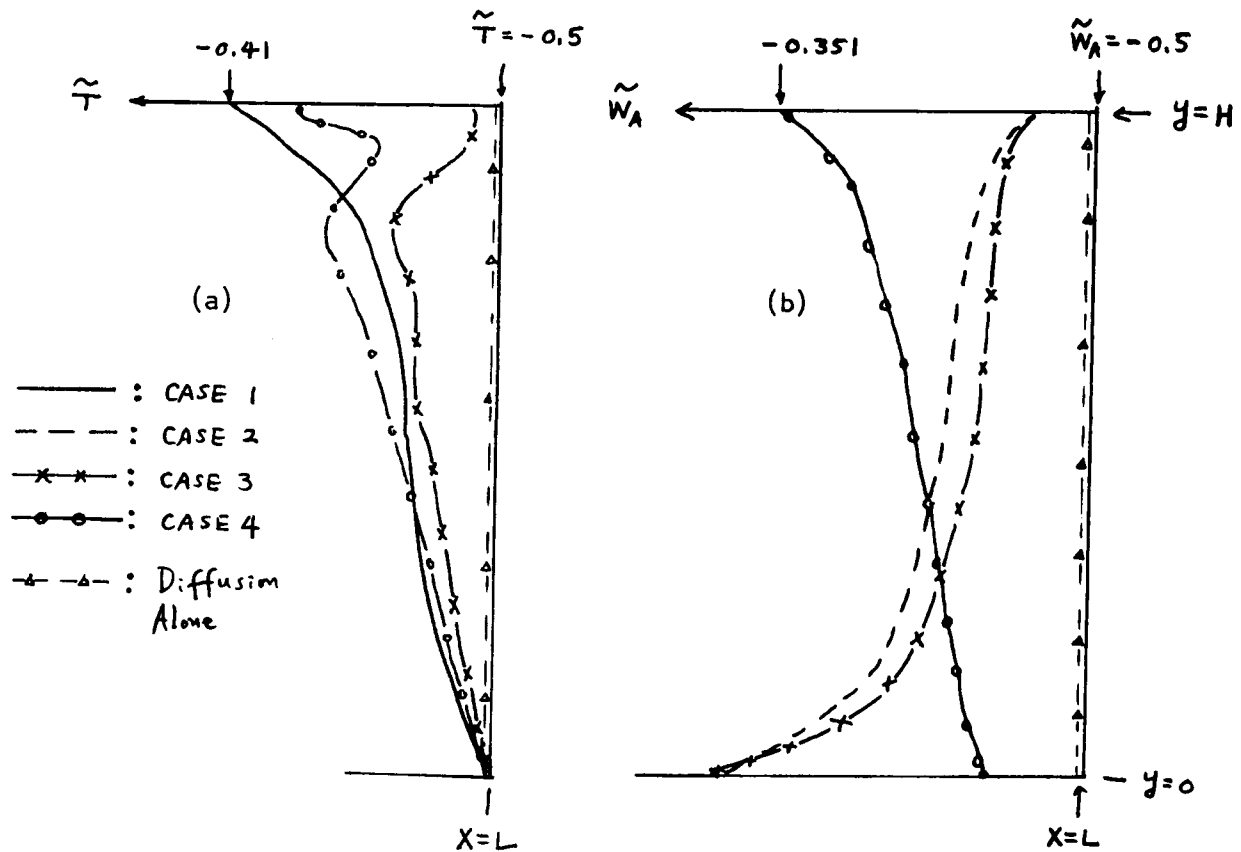


Figure 16. Temperature and mass concentration profiles along the vertical coordinate at the control volumes next to the right vertical surface

V. CONCLUSIONS AND RECOMMENDATIONS

Numerical simulations of thermal and solutal buoyancy driven convections in a rectangular cavity are performed by a numerical model based on the SIMPLE algorithm. Physical parameters are chosen to represent a possible crystal growth from solution.

Numerical results for a pure thermal convection were found to agree reasonably well with a known solution. Numerical results for a pure solutal convection also agree well with an analytic solution in terms of the average Sherwood number. However, the velocity field for the pure solutal convection exhibits a peculiar feature which can not be explained. Relatively large solutal Rayleigh number ($1.67E+10$) and an extremely large Schmidt number (2140) combination might have produced the nonphysical solutions. This has to be checked more carefully through further numerical experimentations.

Overall energy and mass transfer rates are seen to depend strongly on the interactions between the thermal and solutal effects. These interactions are highly nonlinear and the steady-state conditions may not exist for certain combined convections. To arrive at the more conclusive and quantitative correlations, however, experimental investigations covering wide range of nondimensional parameters are required.

To investigate the double-diffusive effects on the flow, a non-uniform initial solutal distribution in the cavity is needed before the commencement of heat transfer from side walls. (The initial solute concentration was assumed constant for present analysis.) This can be easily accomplished by assigning any non-uniform solute distribution in the cavity.

After performing the recommended refinements and verifications as discussed above, one can relax the constraints on the problem formulations, such as the interfacial velocity, segregation effects and the temperature boundary conditions.

ORIGINAL PAGE IS
OF POOR QUALITY

REFERENCES

1. Ostrach, Simon, "Fluid Mechanics in Crystal Growth-The 1982 Freeman Schler Lecture," J. Fluid Eng., Vol 105, 5-20, 1982.
2. Ostrach, Simon, "Low-Gravity Fluid Flows," Ann. Rev. Fluid Mech., Vol. 14, 313-345, 1982.
3. Extremet, G., Roux B., Bontoux P., and Elie F., "Two-dimensional Model for Thermal and Solutal Convection in Multizone Physical Vapor Transport," J. Crystal Growth, Vol. 82, 761-775, 1987.
4. Napolitano, L. G., "Recent Advances in Microgravity Fluid Dynamics," Annal New York Academy of Science, 278-298, 1983.
5. Patankar, S. V., Numerical Heat Transfer and Fluid Flow, McGraw-Hill, 1980.
6. Han, S. M., "A Generalized Implicit Finite Difference Method for Transient Analysis of Compressible and Incompressible Fluid Flows" Numerical Methods for Fluid Transient Analysis, ASME FED-Vol 4, 17-21, 1983.
7. Han, S. M., "A Transient Numerical Analysis of High Rayleigh Number Convection in a Differentially Heated Square Cavity," ASME Paper 84-HT-57, 1984.
8. Bejan, A., Convection Heat Transfer, Wiley and Sons, 1984.
9. Patterson, J. and Imberger, J., "Unsteady Natural Convection in a Rectangular Cavity," J. Fluid Mech., Vol. 100, Part 1, 65-80, 1980.
10. Turner, J. S., "Double-Diffusive Phenomena," Ann. Rev. Fluid Mech., Vol. 6, 37-56, 1974.
11. Gebhart, B. and Pera, L., "The Nature of Vertical Natural Convection Flows Resulting From the Combined Buoyancy Effects of Thermal and Mass Diffusion," Int. J. Heat Mass Transfer, Vol. 14, 2025-2050, 1971.